Macromolecules

ARTICLE

pubs.acs.org/Macromolecules

Dewetting on Curved Interfaces: A Simple Route to Polymer Nanostructures

Dian Chen,[†,§] Wei Zhao,[†,§] Dongguang Wei,[‡] and Thomas P. Russell*[,†]

[†]Department of Polymer Science and Engineering, University of Massachusetts, Amherst, Massachusetts 01003, United States

[‡]Carl Zeiss NTS LLC, One Corporation Way, Peabody, Massachusetts 01960, United States

Supporting Information

ABSTRACT: The dewetting behavior of polystyrene (PS) films immersed in nonsolvent, ethylene glycol, was investigated at temperatures above the glass transition temperature on planar interfaces and on the walls of cylindrical nanopores where the interfacial interactions were varied. PS nanostructures with different shaped end-caps were produced when the PS nanotubes, confined within the cylindrical nanopores of an anodic aluminum oxide (AAO) membrane, were immersed in ethylene glycol, at 130 °C. This system provides an easy approach for fabricating polymer nanostructures with different shapes that can be used to develop unique confined morphologies for the block copolymers. Poly(styrene-*b*-1,4-butadiene) (PS-*b*-PBD) nanospheres and hemispherically capped nanorods were produced having controlled size with different morphologies within the nanostructures.

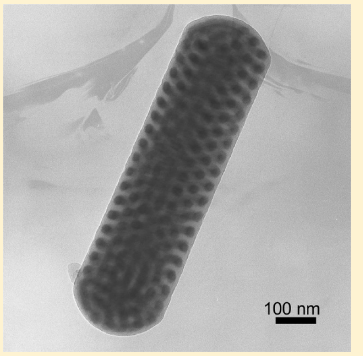

INTRODUCTION

It is well-known that dewetting is an important phenomenon which has direct impact on many industrial processes, such as oil recovery, lubrication, and surface modification.[1] Previous work on the dewetting of polymer films has focused primarily on planar surfaces where, if the spreading coefficient S, defined as $S = \gamma_{gs} - \gamma_{gl} - \gamma_{ls}$, is negative and the film thickness is below a critical value, e_c, a fluid will dewet on a planar solid surface;[2−5] γ_{gs}, γ_{gl}, and γ_{ls} are the air−substrate, air−liquid, and liquid−substrate interface or surface tensions, respectively. There has been less attention paid to curved surfaces, as is the case for the inner walls of a cylindrical pore,[6,7] despite its relevance to the drying of fluids in porous materials. Callegari et al. developed theoretical arguments describing the dewetting of liquid films deposited inside nonwettable and wettable capillaries[6] and investigated water−glycerol solutions experimentally.[7] The film thickness was found to be the key parameter in defining the mechanism by which dewetting occurred. For polymers under cylindrical confinement, Rayleigh instabilities have been observed for poly(methyl methacrylate) (PMMA),[8] PS,[9] and PMMA/PS blends,[10] when heated above their glass transition temperatures (T_g). However, the wetting of thin polymer films inside cylindrical nanopores has not been discussed.

Anodic aluminum oxide (AAO) membranes, widely used as templates for the fabrication of polymer-based nanostructures, including nanotubes,[11,12] nanorods,[13−16] mesoporous nanostructures,[17−19] and vesicles,[20] are an ideal platform to study dewetting. The nanopores in AAO membranes characteristically have a well-defined size (ranging from 8 to 500 nm diameter, depending on the anodization conditions) with a narrow pore size distribution that are arranged in a hexagonal array.[21] The surface properties can also be tuned by chemically modifying the surface, taking advantage of hydroxyl groups on the surface of the walls.[22] Polymer thin films can easily be deposited on the walls of cylindrical nanopores by solvent casting,[8,10,17,20] where the film thickness can be controlled by the solution concentration.[8,23]

Here, we present a study on the dewetting of thin polymer films confined within these nanoscopic cylindrical pores where the surface properties of the walls were changed. To induce dewetting, as opposed to a Rayleigh instability, a small molecule liquid, ethylene glycol (a nonsolvent for the polymer), was introduced to replace air, replacing surface energies with interfacial energies, which significantly decreases instabilities in the thin films. PS films with different thickness were coated onto the walls of the cylindrical nanopores of AAO membranes by varying the solution concentration. This forms what are essentially nanotubes of PS within the AAO membrane. The AAO membranes coated with the PS nanotubes were immersed in ethylene glycol at 130 °C, a temperature well-above the T_g (∼100 °C) of PS, to impart mobility and induce dewetting. Because of the cylindrical confinement, the dewetting process generated polymer nanospheres and nanorods with well-controlled size. The shape and size of the PS nanostructures could be modified by controlling the surface properties of the AAO membrane and the thickness of the PS nanotubes.

Block copolymers (BCPs) have attracted significant attention due to their ability to self-assemble into arrays of nanoscopic microdomain morphologies that can be used as etching masks in

Received: July 4, 2011
Revised: August 23, 2011
Published: September 21, 2011

lithography[24] and patterning tools for nanoelectronics,[25,26] high-density storage,[27] and photonic materials.[28,29] It is well-known that simple AB diblock copolymers microphase separate to form lamellar, gyroid, cylindrical, and spherical nanostructures depending on their composition and the segmental interactions.[30,31] When BCPs are confined within hard templates with different geometries and sizes, confining environments strongly affect the final morphologies that can be different from the morphologies found in the bulk.[32−34]

By using the same method (solution infiltration), the walls of the nanopores in the AAO membrane were coated with a block copolymers, PS-*b*-PBD, instead of PS. The membrane with PS-*b*-PBD film inside was immersed in ethylene glycol at 130 °C, above the T_g of both the PS and PBD blocks. Ethylene glycol is a nonsolvent for both blocks, but preferentially wets the hydrophilic surface of the AAO membrane. This causes a dewetting of the BCP thin film and subsequent formation of BCP nanospheres and nanorods. The BCP microphase separates within the nanostructures, forming unique 2-D or 3-D morphologies, as a result of the confinement, that depended on the molecular weight and composition of the BCPs. Moreover, the nanorods all have hemispherical end-caps, which is rarely seen,[14] opening opportunities to study morphological transitions.

While polymeric nanoparticles have unusual mechanical, optical, and thermal properties,[35] it remains a challenge to fabricate nanoparticles with controlled composition, size, and shape. The process described here is simple and enables studies on the fundamental science underpinning dewetting and the fabrication of polymer-based nanostructures.

Table 1. Material Properties of PS-*b*-PBD Diblock Copolymers

code	M_n (PS) (kg/mol)	M_n (PBD) (kg/mol)	$f_{PBD}{}^V$	bulk morphology	period (nm)
SBD_l	19.9	22	0.558	lamella	32.9
SBD_c	35	11	0.264	cylinder	34.5
SBD_s	30.5	5.5	0.171	sphere	19.9

EXPERIMENTAL SECTION

Materials. PS (M_n = 25.7 kg/mol, PDI = 1.1) and all three of the PS-*b*-PBD diblock copolymers were purchased from Polymer Source Inc. The details of these copolymers are given in Table 1. Small-angle X-ray scattering (SAXS) is used to confirm the bulk morphologies and measure the periods of the BCPs. To calculate volume fraction for PBD block, density values of 1.05 and 0.92 g/cm^3 are used for PS and PBD block, respectively. AAO membranes with two different nanopore diameters were used. One was purchased from Whatman and has average pore diameters of ∼200 nm and thickness of ∼60 μm (c-AAO). The other was prepared using a well-established two-step anodization process.[21] The electrolyte solution used was 0.3 M oxalic acid which was maintained at 17 °C. The anodization was taken out using constant voltage of 40 V on chemically polished aluminum sheets and generated 40−45 nm diameter nanopores with a length of ∼100 μm in the aluminum oxide layer (h-AAO). All the other chemicals, including oxalic acid (powder), perchloric acid (70% aqueous solution), aluminum (99.99% purity), sodium hydroxide (pellet), ethylene glycol, and toluene, were purchased from Sigma-Aldrich and used as received.

Preparation of PS or BCP Nanostructures. PS or PS-*b*-PBD nanotubes were fabricated inside AAO membrane by solution infiltration as previously described.[8,10,17,20] The AAO membrane with PS or PS-*b*-PBD nanotubes inside was immersed into ethylene glycol at 130 °C and annealed for 10 min to induce the dewetting. After removal from ethylene glycol and quenching to room temperature, the AAO membrane was dissolved in sodium hydroxide (NaOH) aqueous solution (5 wt %) to release the nanostructures, which were filtrated and washed with DI water for three times, and then dried in ambient overnight for further characterization.

Characterization. Bright field transmission electron microscope (TEM) studies were conducted with a JEOL 2000 FX TEM operated at an accelerating voltage of 200 kV. The samples were placed onto Formvar-coated copper grids and, if necessary, selectively stained by osmium tetroxide (OsO_4, 2% aqueous solution, purchased from Electron Microscopy Science). The images of PS dewetting procedure were taken by the tensiometer (OCA 20, Future Digital Scientific Co., Garden City, NY).

Tomography was also used to investigate the nanostructures, which was conducted on Zeiss Libra 120 energy filtering TEM equipped with a

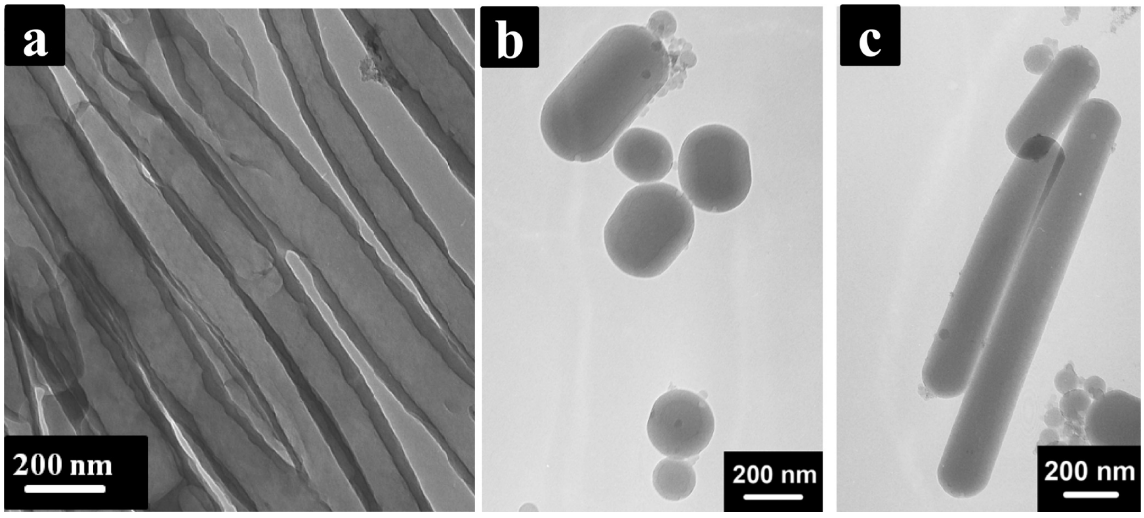

Figure 1. Electron micrographs of PS (25.7K) nanotubes under cylindrical confinement before and after heating in ethylene glycol: (a) TEM image of PS nanotubes prepared using the AAO membrane as a template, (b) TEM image of PS nanospheres, and (c) TEM image of PS nanorods after heating in ethylene glycol for 10 min. All the samples were prepared using c-AAO membrane (pore diameter ∼200 nm). The initial polymer solution concentration is 1 wt %.

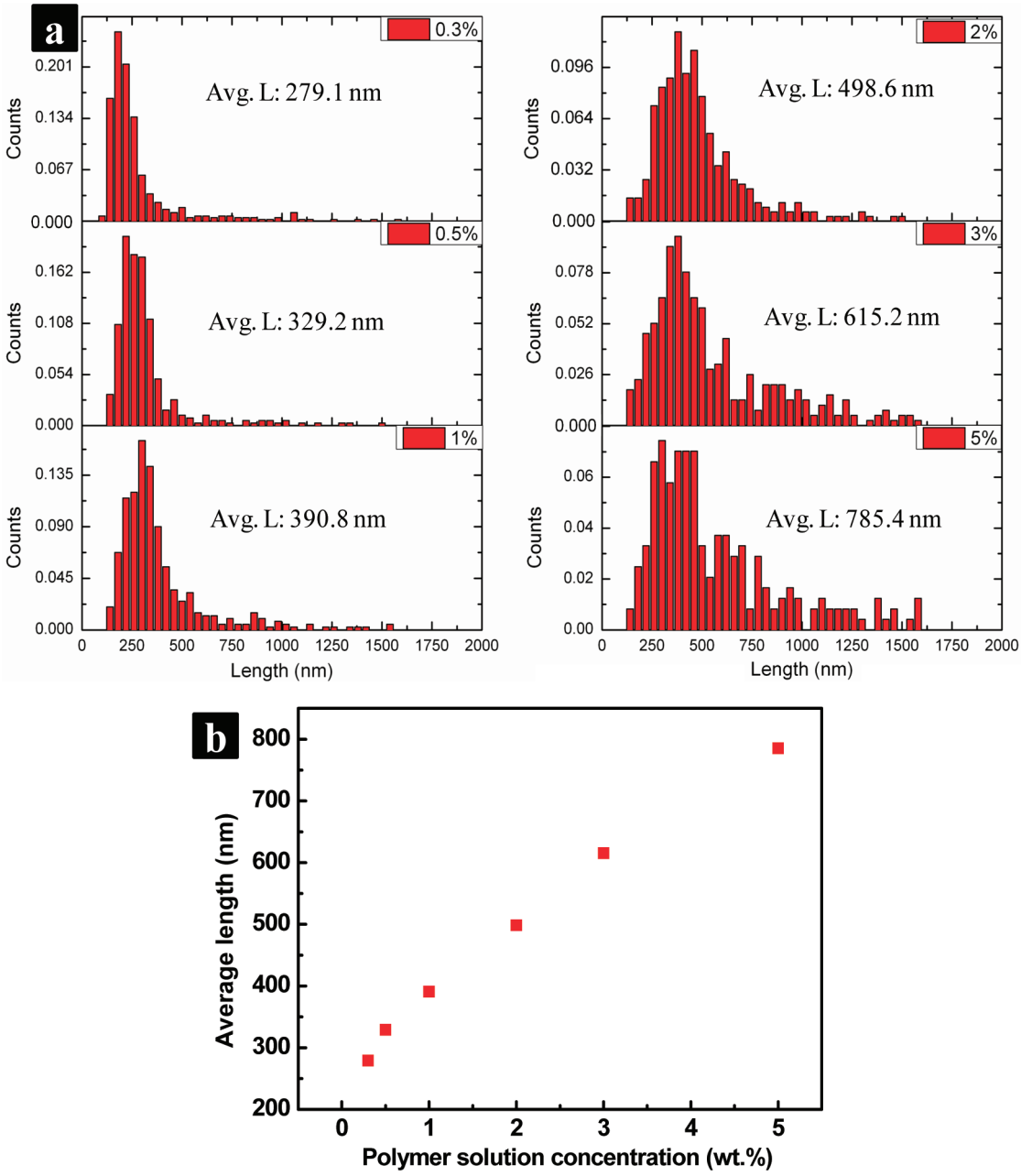

Figure 2. (a) Average length distribution of polymer (PS 25.7K) nanostructures generated at six different initial polymer solution concentrations: 0.3, 0.5, 1, 2, 3, and 5 wt %. All the samples were prepared using c-AAO membrane (pore diameter ~200 nm). (b) Plot of "average length" vs "polymer solution concentration".

LaB6 emitter, an in-column energy filter (electron energy loss spectrometer), and a 2K × 2K SSCCD camera. All images were recorded at 120 kV under zero loss filtered with an energy slit with of 30 eV. The tilt series was acquired from −65° to +65° with an incremental step of 1°. The image stack of 131 images was then aligned against the tilting axis. IMOD software is employed for reconstruction of a tomography movie from the tilt series.

RESULTS AND DISCUSSION

We begin with PS (25.7 K) nanotubes, as shown in Figure 1a, fabricated within the cylindrical nanopores of AAO membranes generated by the capillary filling of polymer solutions (1 wt %) into the membranes followed by solvent evaporation. The thin layer of PS deposited on the walls of the nanopores were then exposed to a nonsolvent, ethylene glycol, and heated to 130 °C, which is above the T_g of PS, whereupon dewetting occurred within the cylindrical nanopores, producing polymeric nanostructures (Figure 1b,c). Solid PS nanospheres and nanorods with hemispherical end-caps were produced with median diameters equal to the average diameter of the cylindrical nanopores in the AAO membrane. This simple process is applicable to many other polymer−solvent pairs, as long as the polymer is not soluble in the solvent and the T_g of the polymer is lower than the boiling point of the solvent.

The size of nanostructures generated can be tuned by changing either the diameter of the cylindrical nanopores in the AAO

dx.doi.org/10.1021/ma2015276 |*Macromolecules* 2011, 44, 8020–8027

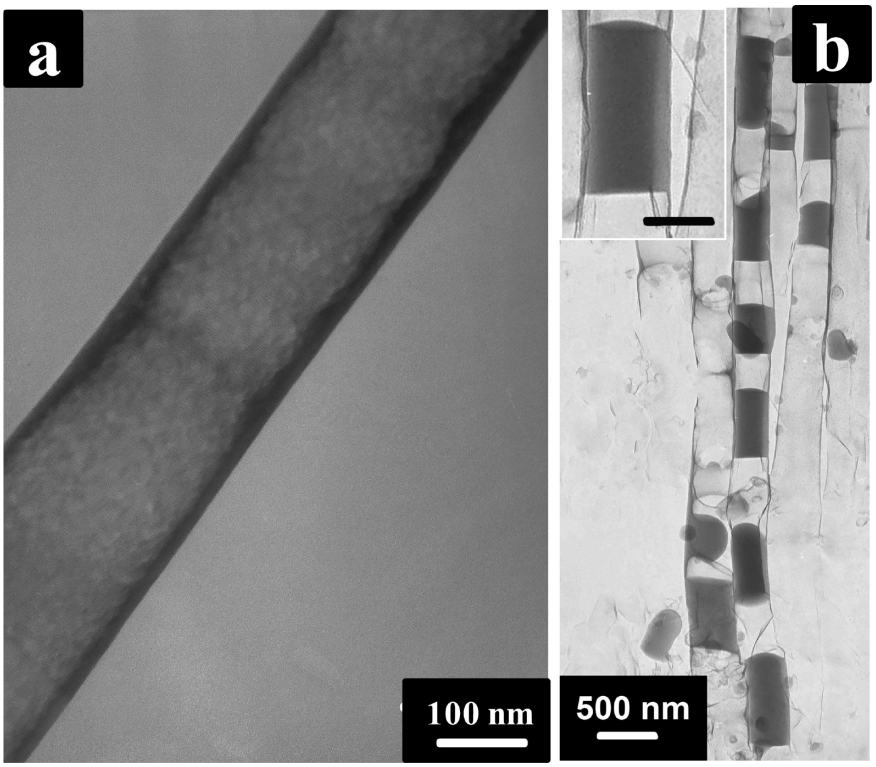

Figure 3. Electron micrographs of PS (25.7K) nanostructures generated within A-CNs: (a) A-CNs generated from a PAN precusor using c-AAO (pore diameter ~200 nm) as the template; (b) TEM image of PS nanostructures generated after PS nanotubes were heated within the A-CNs in ethylene glycol for 10 min. Inset: magnified view of one PS nanorod (with scale bar representing 250 nm).

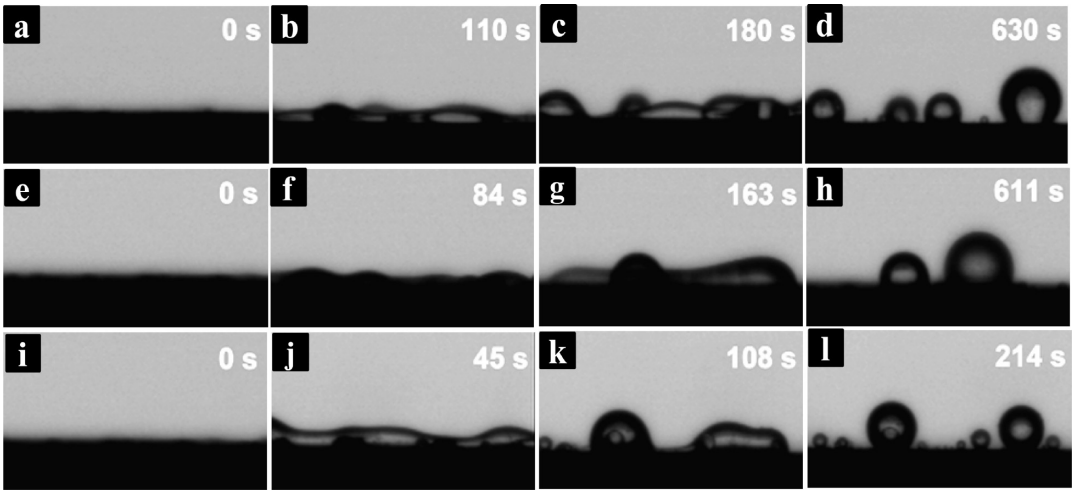

Figure 4. Telescopic graphs of PS (25.7K) films undergoing dewetting on different substrate while heated in ethylene glycol at 130 °C for different periods of time: (a–d) silicon wafer coated with aluminum oxide; (e–h) silicon wafer coated with amorphous carbon; (i–l) silicon wafer with a layer of silicon oxide.

membrane or the concentration of the polymer solution used to fill the membranes, since this will change the total amount of polymer deposited on the nanopore walls. The influence of the solution concentration is shown in Figure 2 where six different concentrations of PS in toluene, ranging from 0.3 to 5 wt %, were used. All samples were treated identically where the PS nanotubes, confined within the cylindrical nanopores, were heated in ethylene glycol at 130 °C for 10 min. As shown in Figure 2b, the average length of the PS nanostructures increased with increasing polymer solution concentration.

The influence of the surface properties of the cylindrical nanopores in the AAO membrane was also studied by first producing amorphous carbon nanotubes (A-CNs) within the cylindrical nanopores. As shown previously by Chen et al., A-CNs are produced by coating the walls of the nanopores with the polyacrylonitrile (PAN), an amorphous carbon precursor,

followed by a two-step pyrolysis,[22] as shown in the Figure 3a. The surface properties of the A-CNs are markedly different from that of aluminum oxide and, as such, provide a very easy means of varying the surface properties of the nanotubes with the surety that the surface properties are absolutely uniform. A 1% solution of PS in toluene was drawn into the A-CNs by capillary action, the solvent was evaporated, and the PS film, deposited on the inner wall of the A-CNs, was dried under vacuum at room temperature. Subsequently, ethylene glycol was drawn into the PS-coated A-CNs and heated to 130 °C for 10 min. The transparency of the A-CNs to electrons enabled the characterization of the nanostructures produced by transmission electron microscopy (TEM) without removing the nanostructures from the A-CNs. As seen in Figure 3b, PS dewetted inside the A-CNs and PS nanostructures with different end shapes (flat instead of hemispherical) were produced (Figure 3b). By comparing the expanded view in the inset of Figure 3b with the nanorods in Figure 1c, it is evident that the shapes of the nanorod ends are different.

To understand how the PS nanostructures with differently shaped ends were generated, experiments were performed in real time for PS films (~10 μm in thickness) on flat silicon wafers where the surface properties were varied (including silicon wafers with the native oxide surface layer, with an amorphous carbon coating, and with an aluminum oxide coating). The different substrates, coated with PS films, were immersed in ethylene glycol at 130 °C and kept stationary to minimize perturbations due to flow. Dewetting occurred and the PS films ruptured into droplets of different size, depending on the initial film thickness and surface properties of the substrates. As shown in Figure 4, dewetting occurred where the flat film developed undulations that increased in magnitude and eventually led to the formation of droplets. Subsequently, the droplets assumed a hemispherical shape, typically seen with dewetting processes in air, where a contact angle could be measured. The contact angles measured for the aluminum oxide, amorphous carbon and silicon oxide substrates were 132.4°, 113.4°, and 144.2°, respectively.

Based on these results, a mechanism can be proposed for the generation of nanospheres and nanorods inside the cylindrical nanopores, illustrated in Scheme1. When the PS nanotube coated on the walls of the AAO membrane is immersed in ethylene glycol at temperatures above the T_g of PS, the nonfavorable interactions of PS with the ethylene glycol and the slightly nonfavorable interactions of the PS with the AAO and the favorable interactions of ethylene glycol with the AAO lead to an instability of the PS film. This induces undulations on the surface of the film that increase in amplitude with time (Scheme 1b). Eventually, the amplitude of the undulations is sufficiently large, comparable to the thickness of the film, that the ethylene glycol makes contact with the AAO, forcing a dewetting of the PS film. However, unlike dewetting on flat substrates, where there is unlimited space normal to the film surface, within the confines of the nanopores the undulations are comparable to the diameter of the nanopores and lead to the formation of a solid plug of PS within the nanopores (Scheme 1c). The length of the plug along the axis of the nanopore will continue to increase until dewetting ceases and the ends of the plugs, now nanorods, will assume contact angles in accordance to Young's equation. Obviously, the shape of the ends of the nanorods can be controlled by changing the emersion fluid or the surface energy of the nanopore walls. The differences in the length of the nanorods arise from differences in the initial thickness of the film deposited on the walls of the nanopores and the characteristic wavelength of the undulations (Scheme 1d).

Scheme 1. Cross Sections of Schematics for the Formation of Polymer Nanostructures (Nanospheres and Nanorods) inside the Cylindrical Nanopores of AAO Membrane[a]

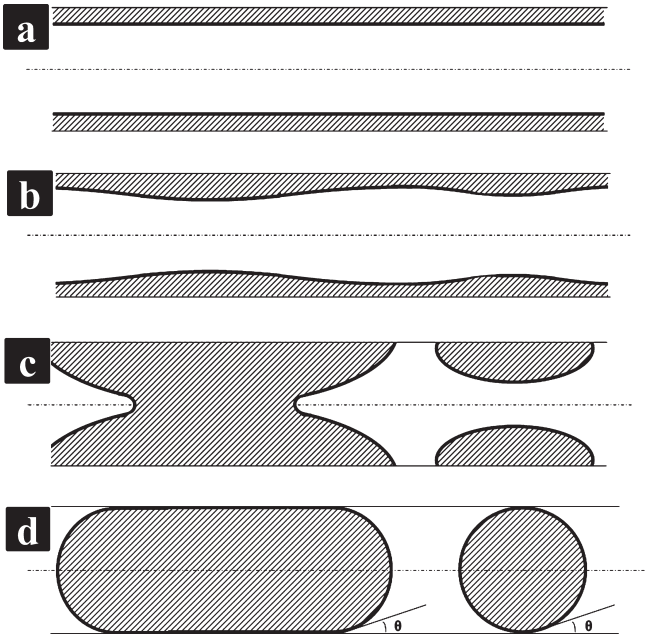

[a] (a) Nanotube with relative uniform thickness; (b) undulations begin to appear after certain time of annealing (above T_g of polymer) in contact with nonsolvent; (c) undulations grow in amplitude, break along the direction of cylinder axis, and merge in direction normal to the cylinder axis; (d) reshape of the merged polymer materials, which is determined by the specific interactions between the polymer−nonsolvent, nonsolvent−cylinder surface, and polymer−cylinder surface.

The physical properties of PS-*b*-PBD diblock copolymers are given in Table 1. The morphologies of the PS-*b*-PBD nanospheres/nanorods fabricated using the AAO membranes were investigated by TEM. Figure 5 shows the morphology in nanospheres/nanorods for the cylinder forming SBD_c. OsO_4 was used to selectively stain the PBD block; consequently, the dark microdomains can be assigned to PBD, while the unstained PS microdomains are gray. Common to all the morphologies is that PS, which interacts more favorably with the ethylene glycol, segregates to the walls of the nanopores, forming a layer of PS at this interface. This is in keeping with observations by others.[20,36,37] A short nanorod is shown in Figure 5a, where helical PBD microdomains can be seen (most clearly near the edge). Because of the relative large diameter of the nanorods (in comparison to the bulk period), several layers of helices form inside the nanorods with their axes parallel to the nanorod axis, packed in a hexagonal manner. The packing symmetry can be derived from the hexagonal array of black dots inside the rectangular dashed region, which come from the particular projection angle of the helices relative to the image plane. The three-dimensional microstructures were reconstructed and visualized by transmission electron microtomography (see movie in Supporting Information). This result is similar to the results of Jeon et al. with blends of PS-*b*-PBD and PS, where hexagonally packed helices preferentially aligned along the longer axis of the slightly ellipsoidal nanoparticles.[36] Similar morphologies were observed in the longer nanorods, as shown in Figure 5b. Another common feature of the morphologies is that the PBD helices close to the

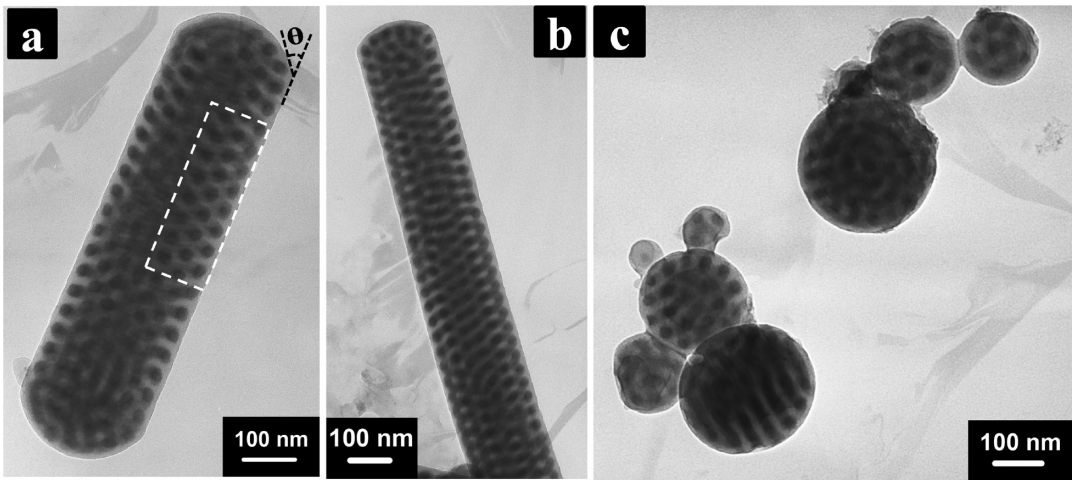

Figure 5. TEM images of nanostructures generated from SBD_c nanotubes prepared in c-AAO membrane (pore diameter ~200 nm) after heating in ethylene glycol at 130 °C for 10 min: (a) short nanorod, (b) long nanorod, and (c) nanospheres. OsO_4 was used to selectively stain PBD microdomains, which appear dark in images while PS microdomains remain gray. Sample was prepared by dropping nanostructure suspension onto TEM grid.

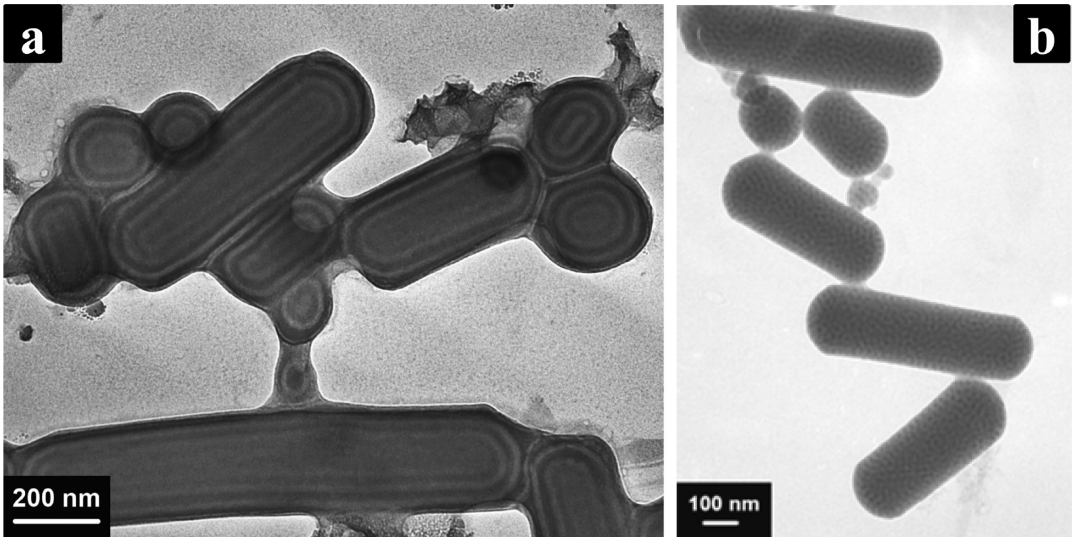

Figure 6. TEM images of nanostructures generated from (a) SBD_l and (b) SBD_s nanotubes prepared in c-AAO membrane (pore diameter ~200 nm) after heating in ethylene glycol at 130 °C for 10 min. OsO_4 was used to selectively stain PBD microdomains, which appear black in images while PS microdomains remain gray. Sample was prepared by dropping nanostructure suspension onto a TEM grid.

hemispherical ends of the nanorods become less aligned and even some defects can be seen. This indicates that the helical morphology is not compatible or commensurate with the spherical symmetry forced by the shape of the end-cap. In keeping with this end effect, the ordering in spherical nanoparticles is not perfect, as shown in Figure 5c, which is consistent to the situation of their small size nanoparticles in Jeon's experiments.[36]

Under the same conditions nanoparticles of bulk lamella- and sphere-forming PS-*b*-PBDs can easily be fabricated, as shown in Figure 6. The morphology for bulk lamella-forming SBD_l (Figure 6a) is exclusively an onion-like structure, which was shown to be more favorable upon long-time thermal annealing.[38] Also, the outer layers of these nanospheres and nanorods are exclusively PS, which is consistent with the results for SBD_c shown above. As for the morphology of bulk sphere forming SBD_s, confinement effects and mismatches in the symmetries of the BCP morphology and the geometry of the nanorods are minimal, and as such, a bcc packing of the spherical microdomains is observed (Figure 6b).[32]

As stated above, one additional advantage in using the AAO membranes for preparing the BCP nanoparticles is size control. By changing the diameter of the nanopores of AAO membrane, the diameter of the nanorods can be changed from 20 to 500 nm. Using an AAO membrane with an average pore diameter of ~40–45 nm, the nanostructures shown in Figure 7 were obtained for SBD_c copolymer. The ends of the nanorods retained the hemispherical shape, and the contact angles ($180°-\theta$), shown in Figure 7a, are identical to those in Figure 5a, reflecting the segregation of the PS to the walls. In Figure 7a, PS-*b*-PBD single-helix (triple arrow), double-helix (double arrow), and torus-like (single arrow) morphologies were clearly observed. In the ~50 nm diameter nanospheres shown in Figure 7b, the helical structure can still be observed, but not as well ordered as that in the nanorods, due to the mismatch in the symmetries.

dx.doi.org/10.1021/ma2015276 |*Macromolecules* 2011, 44, 8020–8027

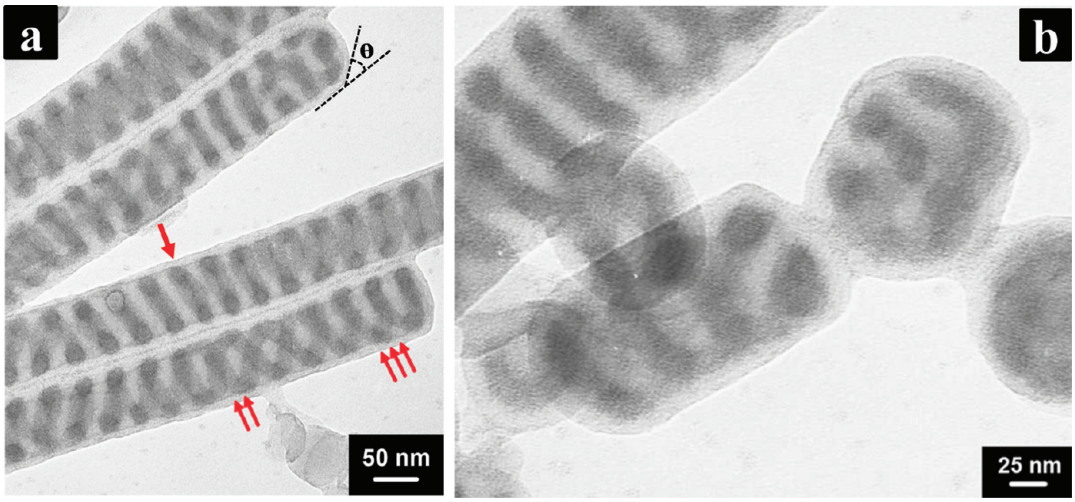

Figure 7. TEM images of nanostructures generated from SBD_c nanotubes prepared in h-AAO membrane (pore diameter ~45 nm) after heating in ethylene glycol at 130 °C for 10 min: (a) long nanorods; (b) short nanorods and nanospheres.

CONCLUSION

The dewetting behavior of PS films on flat and curved surfaces in the presence of ethylene glycol was investigated at 130 °C, above the glass transition temperature of PS. Polymer nanostructures (nanospheres and nanorods) with different end shapes and sizes could be generated and controlled by changing the surface properties of the cylindrical nanopores and the initial film thickness, offering a facile approach to the fabrication of nanostructures with controlled composition, size, and shape. These nanostructures also exhibit novel morphologies, not accessible in bulk systems, due to confinement effects, incommensurability between the symmetry of the BCP and geometric shape of the nanoparticles, and the preferential segregation of components to surface and interfaces.

ASSOCIATED CONTENT

Supporting Information. Transmission electron microtomography. This material is available free of charge via the Internet at http://pubs.acs.org.

AUTHOR INFORMATION

Corresponding Author

*E-mail: russell@mail.pse.umass.edu.

Author Contributions

§These authors equally contributed to this work.

ACKNOWLEDGMENT

This work was supported by the U.S. Department of Energy (DOE), Office of Basic Energy Science, and the NSF-supported Materials Research Science and Engineering Center at the University of Massachusetts Amherst.

REFERENCES

(1) de Gennes, P. G.; Brochard-Wyart, F.; Quéré, D. *Capillarity and Wetting Phenomena: Drops, Bubbles, Pearls, Waves*; Springer Press: Berlin, 2004.

(2) Xie, R.; Karim, A.; Douglas, J. F.; Han, C. C.; Weiss, R. A. *Phys. Rev. Lett.* **1998**, *81*, 1251–1254.

(3) Stange, T. G.; Evans, D. F.; Hendrickson, W. A. *Langmuir* **1997**, *13*, 4459–4465.

(4) Herminghaus, S.; Jacobs, K.; Mecke, K.; Bischof, J.; Fery, A.; Ibn-Elhaj, M.; Schlagowski, S. *Science* **1998**, *282*, 916–919.

(5) Luo, C. X.; Xing, R. B.; Zhang, Z. X.; Fu, J.; Han, Y. C. *J. Colloid Interface Sci.* **2004**, *269*, 158–163.

(6) Callegari, G.; Calvo, A.; Huhn, J. P.; Brochard-Wyart, F. *Langmuir* **2002**, *18*, 4795–4798.

(7) Callegari, G.; Calvo, A.; Hulin, J. P. *Eur. Phys. J. E* **2005**, *16*, 283–290.

(8) Chen, J. T.; Zhang, M. F.; Russell, T. P. *Nano Lett.* **2007**, *7*, 183–187.

(9) Mei, S. L.; Feng, X. D.; Jin, Z. X. *Macromolecules* **2011**, *44*, 1615–1620.

(10) Chen, D.; Chen, J. T.; Glogowski, E.; Emrick, T.; Russell, T. P. *Macromol. Rapid Commun.* **2009**, *30*, 377–383.

(11) Steinhart, M.; Wendorff, J. H.; Greiner, A.; Wehrspohn, R. B.; Nielsch, K.; Schilling, J.; Choi, J.; Gosele, U. *Science* **2002**, *296*, 1997–1997.

(12) Steinhart, M.; Wehrspohn, R. B.; Gosele, U.; Wendorff, J. H. *Angew. Chem., Int. Ed.* **2004**, *43*, 1334–1344.

(13) Moon, S. I.; McCarthy, T. J. *Macromolecules* **2003**, *36*, 4253–4255.

(14) Zhang, M. F.; Dobriyal, P.; Chen, J. T.; Russell, T. P.; Olmo, J.; Merry, A. *Nano Lett.* **2006**, *6*, 1075–1079.

(15) Feng, X. D.; Jin, Z. X. *Macromolecules* **2009**, *42*, 569–572.

(16) Chen, J. T.; Chen, D.; Russell, T. P. *Langmuir* **2009**, *25*, 4331–4335.

(17) Chen, D.; Park, S.; Chen, J. T.; Redston, E.; Russell, T. P. *ACS Nano* **2009**, *3*, 2827–2833.

(18) Wang, Y.; Gosele, U.; Steinhart, M. *Nano Lett.* **2008**, *8*, 3548–3553.

(19) Wang, Y.; Tong, L.; Steinhart, M. *ACS Nano* **2011**, *5*, 1928–1938.

(20) Zhao, W.; Chen, D.; Hu, Y. X.; Grason, G. M.; Russell, T. P. *ACS Nano* **2011**, *5*, 486–492.

(21) Masuda, H.; Fukuda, K. *Science* **1995**, *268*, 1466–1468.

(22) Chen, J. T.; Shin, K.; Leiston-Belanger, J. M.; Zhang, M. F.; Russell, T. P. *Adv. Funct. Mater.* **2006**, *16*, 1476–1480.

(23) Chen, J. T.; Zhang, M. F.; Yang, L.; Collins, M.; Parks, J.; Avallone, A.; Russell, T. P. *J. Polym. Sci., Part B: Polym. Phys.* **2007**, *45*, 2912–2917.

(24) Park, M.; Harrison, C.; Chaikin, P. M.; Register, R. A.; Adamson, D. H. *Science* **1997**, *276*, 1401–1404.

(25) Lopes, W. A.; Jaeger, H. M. *Nature* **2001**, *414*, 735–738.

(26) Hu, Y. X.; Chen, D. A.; Park, S.; Emrick, T.; Russell, T. P. *Adv. Mater.* **2010**, *22*, 2583–2587.
(27) Hawker, C. J.; Russell, T. P. *MRS Bull.* **2005**, *30*, 952–966.
(28) Urbas, A.; Fink, Y.; Thomas, E. L. *Macromolecules* **1999**, *32*, 4748–4750.
(29) Yoon, J.; Lee, W.; Thomas, E. L. *Nano Lett.* **2006**, *6*, 2211–2214.
(30) Fredrickson, G. H.; Bates, F. S. *Annu. Rev. Mater. Sci.* **1996**, *26*, 501–550.
(31) Matsen, M. W.; Schick, M. *Phys. Rev. Lett.* **1994**, *72*, 2660–2663.
(32) Dobriyal, P.; Xiang, H. Q.; Kazuyuki, M.; Chen, J. T.; Jinnai, H.; Russell, T. P. *Macromolecules* **2009**, *42*, 9082–9088.
(33) Wu, Y. Y.; Cheng, G. S.; Katsov, K.; Sides, S. W.; Wang, J. F.; Tang, J.; Fredrickson, G. H.; Moskovits, M.; Stucky, G. D. *Nature Mater.* **2004**, *3*, 816–822.
(34) Li, L.; Matsunaga, K.; Zhu, J. T.; Higuchi, T.; Yabu, H.; Shimomura, M.; Jinnai, H.; Hayward, R. C.; Russell, T. P. *Macromolecules* **2010**, *43*, 7807–7812.
(35) Sundberg, D. C.; Durant, Y. G. *Polym. React. Eng.* **2003**, *11*, 379–432.
(36) Jeon, S. J.; Yi, G. R.; Koo, C. M.; Yang, S. M. *Macromolecules* **2007**, *40*, 8430–8439.
(37) Brannan, A. K.; Bates, F. S. *Macromolecules* **2004**, *37*, 8816–8819.
(38) Higuchi, T.; Motoyoshi, K.; Sugimori, H.; Jinnai, H.; Yabu, H.; Shimomura, M. *Macromol. Rapid Commun.* **2010**, *31*, 1773–1778.